Solid−Liquid Interfacial Energy and Melting Properties of Nickel under Pressure from Molecular Dynamics

Fen Luo,[†] Xiang-Rong Chen,*[,†,‡] Ling-Cang Cai,[§] and Guang-Fu Ji[§]

School of Physical Science and Technology, Sichuan University, Chengdu 610064, China, International Centre for Materials Physics, Chinese Academy of Sciences, Shenyang 110016, China, and Laboratory for Shock Wave and Detonation Physics Research, Institute of Fluid Physics, Chinese Academy of Engineering Physics, Mianyang 621900, China

We carried out molecular dynamics (MD) simulations with the quantum-corrected Sutton−Chen (Q-SC) potential to compute the thermal equation of state (EOS), the solid−liquid interfacial energy, and melting properties of nickel. We simulate the melting with two methods, the hysteresis (one-phase) approach and the solid−liquid coexistence (two-phase) approach. These methods strongly reduced the overheating, and their results are in the close proximity over a large range of pressure. The melting temperature at ambient pressure is in accordance with the diamond anvil cell (DAC) experiment values. With a superheating and undercooling method, solid−liquid interfacial energy as a function of pressure is exhibited. Moreover, the thermal EOS has been investigated, and the linear thermal expansivity as a function of temperature has also been obtained successfully.

1. Introduction

The melting property of materials is still an important field of condensed-matter physics. Extensive experimental studies[1−8] and theoretical work[9−19] have been applied to a number of metals. Particularly, for the laser-heated diamond anvil cell (DAC) measurement of the melting curves of transition metals, such as Ni, Ta, Mo, and so on, the melting slopes[4,5,7] (dT/dP) at high pressures are unusually low. As for Ni, several discrepancies in the DAC data[2,4,7] with theoretical data[18] still exist. Lazor et al.[2] and Errandonea et al.[4] applied the laser-heated DAC technique to investigate ultrahigh melting curves. Japel et al.[7] measured the melting curves in a laser-heated DAC and confirmed the key role of *d*-shell electrons in determining melting temperatures. Subsequently, Ross et al.[18] calculated the melting curves of Ni with the free energy model, and their results are much larger than the melting temperatures extrapolated from DAC experiments. To date, data of the melting properties of Ni at high pressures are scarce, and it is unclear whether the abnormal behavior still exists in the high-pressure melting curves of Ni. Hence, the goal of the present investigation is to pay attention to the high-pressure melting of Ni, using molecular dynamics (MD) simulations with the quantum-corrected Sutton−Chen (Q-SC) potential.[20] The Q-SC potential has been successfully applied in many metals.[21,22]

In accurately determining the equilibrium melting point of crystals using the hysteresis (one-phase) approach[10] and the solid−liquid coexistence (two-phase) approach,[23] MD simulations appear to be essential for application. In the first approach, the solid phase is heated until melting, and then the liquid phase is cooled until freezing under various pressures. The melting temperature is deduced from the temperature of the degree of superheating and supercooling. From a theoretical point of view, two-phase MD simulations, which can avoid the superheating effect, provide a very accurate tool to study the melting properties of large systems. In recent years, this method has been successfully applied to many materials, such as Lannard−Jonesium,[24] LiH,[25] MgO and NaCl,[26] GaN,[27] Ne,[28] and so on.

The other intriguing problem is the solid−liquid interfacial energy γ_{sl}. Few theoretical studies of nickel solid−liquid interfacial properties have been reported to date. Hoyt et al.[29] reported $\gamma_{sl} \approx 0.23\ J \cdot m^{-2}$ with the different embedded atom model and the analysis of the capillary wave spectrum. A theoretical result $\gamma_{sl} \approx 0.18\ J \cdot m^{-2}$ was reported by Zykova-Timan et al.[30] Now, we apply the superheating/undercooling method with MD simulations[10] to calculate the solid−liquid interfacial energy of nickel.

The aim of the present work is as follows. First, we propose to compare the hysteresis approach and the two-phase approach to estimate the high-pressure melting line of nickel in MD simulations. Then, we study the thermal equation of state (EOS) and the solid−liquid interfacial energy.

2. Computational Method

2.1. Potential Function. In this work, we have adopted the Q-SC potential as the reference potential. In the Q-SC potential,[20] the total potential energy of the metal is given as follows:

$$U_{tot} = \sum_i U_i = \sum_i \varepsilon \left[\sum_{j \neq i} \frac{1}{2} V(r_{ij}) - c\sqrt{\rho_i} \right] \qquad (1)$$

where $V(r_{ij})$ is a pair potential defined by the following form

$$V(r_{ij}) = \left(\frac{a}{r_{ij}} \right)^n \qquad (2)$$

Accounting for a two-body repulsive interaction between the atoms i and j, ρ_i is a local density accounting for the cohesion associated with atom i defined by

* Corresponding author. E-mail: x.r.chen@tom.com.
[†] Sichuan University.
[‡] Chinese Academy of Sciences.
[§] Chinese Academy of Engineering Physics.

10.1021/je1007058
Published on Web 10/04/2010

$$\rho_i = \sum_{j \neq i} \varphi(r_{ij}) = \sum_{j \neq i} \left(\frac{a}{r_{ij}}\right)^m \quad (3)$$

In eqs 1 to 3, ε sets the overall energy scale, r_{ij} is the distance between the atoms i and j, a is an arbitrary length parameter leading to a dimensionless value for $V(r_{ij})$ and ρ_i, c_i is a dimensionless parameter scaling the attractive term relative to the repulsive term, and n and m are positive integer parameters such that $n > m$. The fitted parameters for Ni[20] are $n = 10$, $m = 5$, $\varepsilon = 0.0073767$ eV, $c = 84.745$, and $a = 3.5157$ Å.

2.2. Molecular Dynamics (MD) Simulations. The calculations were done with the DL_POLY2.17 program.[31] We performed MD simulations of the solid−liquid systems in the Berendsen isothermal−isobaric (normal pressure and temperature, NPT) ensemble.[32] The relaxation times used for the thermostat and barostat are (0.5 and 0.5) ps, respectively. The potential cutoff radius of 9 Å was applied, and the smooth particle-mesh Ewald method[33] was employed with the electrostatic interaction. Integration of the equation of motion has been performed with a time step of 1 fs; the system was equilibrated for a minimum of 6 ps (6000 time steps), and statistical averages of properties such as volumes and energies were computed over the remaining time of the 4 ps (4000 time steps) simulation.

In the two-phase MD simulations, we started with the supercell consisting of 4 × 4 × 8, 5 × 5 × 10, and 6 × 6 × 12 face-centered-cubic (fcc) conventional unit cells corresponding to 512, 1000, and 1728 atoms in the fcc structure, froze the half part of the *z*-coordinates of the cell, and then heated them up to 3000 K (above the melting point) in the microcanonical ensemble (NVE) ensemble to allow the molecules at the contact surface to relax to more stable positions. The single-phase MD simulations started with the fcc Ni crystal of 5 × 5 × 5 cell units, which contains 500 atoms. The single crystal Ni was subjected to incremental heating under the NPT ensemble at a fixed pressure until melting. Similarly, the liquid Ni was followed by the same temperature increment cooling until recrystallization.

2.3. Equilibrium Melting Point. The two-phase MD simulations can be used to obtain the melting temperature T_m.[17,34] In Figure 1a, we show the initial configuration with average number density of the supercell parallel to the solid−liquid interface. The solid phase is identified by periodic oscillations of the density, while the number density of the liquid phase fluctuates randomly with much smaller amplitudes. Under a fixed pressure, when the system temperature is below the melting point, the interfaces will move toward the liquid part (Figure 1b), whereas it moves toward the solid parts above the melting point (Figure 1c). We can judge the melting temperature either below or above the melting point at a fixed pressure by monitoring the moving direction of interfaces from the average number density of the supercell. Then, we narrowed the range of the melting temperature at this pressure. Repeating the above steps, we can obtain the whole melting curve within the applied pressures. To ensure that the system is indeed melting, we can analyze the radical distribution function (RDF) of the atom. In Figure 2, the RDF of the solid is characterized by the pronounced peaks from short to long-range, but many peaks are absent or flattened in the RDF of the liquid.

For the solid−liquid phase transition in a single-component system, supercells with three-dimensional periodic boundaries and NPT ensembles were conducted in the MD simulations. When we heat the perfect single crystal Ni incrementally, a sudden jump in the volume upon melting T_+ can be found. Also, a drop in the volume at T_- in a cooling simulation of liquid Ni can be seen. The volume−temperature ($V-T$) curve (Figure 3) reveals the hysteresis effects for the MD simulations of a solid and a liquid. The equilibrium melting temperature T_m can be deduced from the temperature for the maximum degree of superheating (T_+) and supercooling (T_-)[35,36]

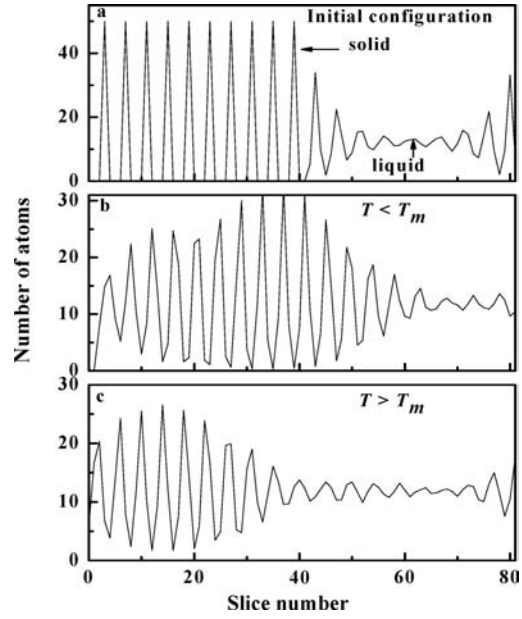

Figure 1. Density profile in a simulation of the solid−liquid coexistence configuration. The solid phase is identified by periodic oscillations of the density, while the density of the liquid phase fluctuates randomly with much smaller amplitudes. (a) The initial configuration, (b) the movement of interfaces toward the liquid part when $T < T_m$, (c) the movement of interfaces toward the solid part when $T > T_m$. The simulation box contained 1000 atoms, and the slice width was 0.419 Å.

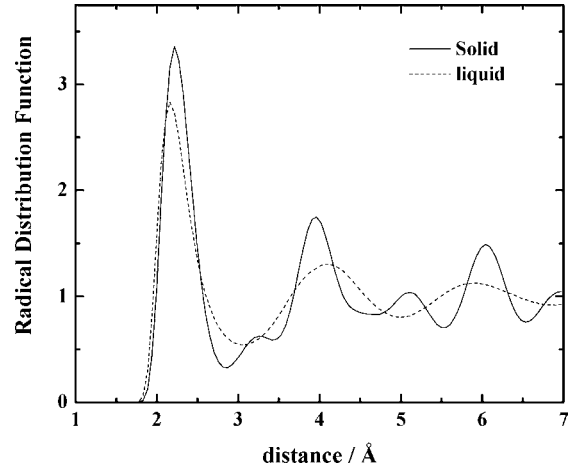

Figure 2. RDF calculated for solid and liquid Ni right before and right after melting.

$$T_m = T_+ + T_- - \sqrt{T_+ T_-} \quad (4)$$

The measurement of solid−liquid interfacial energy γ_{sl} is related to the systematic maximum superheating and supercooling, which is based on classical nucleation.[10] The temperature for the maximum degree of superheating (T_+) and supercooling (T_-) is dependence of the dimensionless nucleation barrier parameter (β) and the heating rate (Q). From the systematic maximum superheating and supercooling, the nucleation barrier parameter is given by

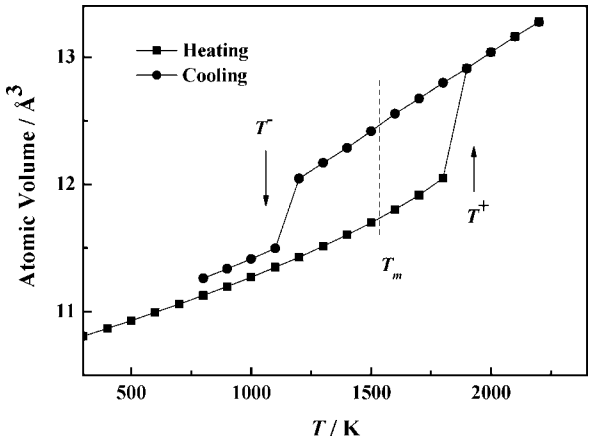

Figure 3. Atomic volume vs temperature during the incremental superheating and undercooling process of nickel. The melting point T_m can be determined from the superheating and supercooling temperatures T^+ and T^-, respectively, using eq 4.

$$\beta = (A_0 - \log_{10} Q)\theta_c(\theta_c - 1)^2 \quad (5)$$

where $A_0 = 59.4$, $b = 2.33$, and Q is normalized by $Q_0 = 1$ K·s^{-1}. The dimensionless temperature $\theta_c = T_+/T_m$ or T_-/T_m, where T_m is the equilibrium melting temperature. If we obtain β, H_m, and T_m, γ_{sl} can be determined by,

$$\gamma_{sl} = \left(\frac{3}{16\pi}\beta k_B T_m \Delta H_m^2\right)^{1/3} \quad (6)$$

where ΔH_m is the enthalpy change per unit volume between the solid and the liquid phases at the melting point. The system was subjected to incremental heating and cooling at a rate of $2 \cdot 10^{12}$ K·s^{-1}, increasing (decreasing) the temperature by 100 K every 10 000 steps. The time step for trajectory integration was 5.0 fs.

3. Results and Discussion

3.1. Melting Properties of Nickel. The melting temperature of nickel as a function of pressure predicted by the coexistence phase method is shown in Figure 4 and is compared with experimental[2−4,7] and theoretical[18] results. For the coexistence phase method, from unit cells corresponding to 512, 1000, and 1728 atoms, we find an increase in the discrepancy in the high-pressure range from the melting curve. For 512 and 1000 atoms, a difference of (12 to 25) % in the range of pressure is shown here. When we adopt 1728 atoms, the results are only a little different with those of 1000 atoms, indicating that convergence of the melting temperature is achieved with the $5 \times 5 \times 10$ supercell of 1000 atoms. The dependence of melting temperature on the number of atoms is related to the dependence of the mean-square displacement on the number of atoms.[37] When the size of the simulation system is sufficiently large, the melting temperature will come to convergence.

The melting temperatures of Ni with 1000 atoms at various pressures are shown in Table 1. The data point of our calculated melting temperature obtained with the $5 \times 5 \times 10$ supercell of 1000 atoms is (1725 ± 50) K, which is in excellent agreement with the experimental result of 1728 K.[3] In the lower pressure range of around (0 to 30) GPa, our melting curves both agree with the DAC values,[2,4,7] but at high pressure our two melting curves all diverge from DAC values with increasing pressure as well as other theoretical results.[18] Since there are little

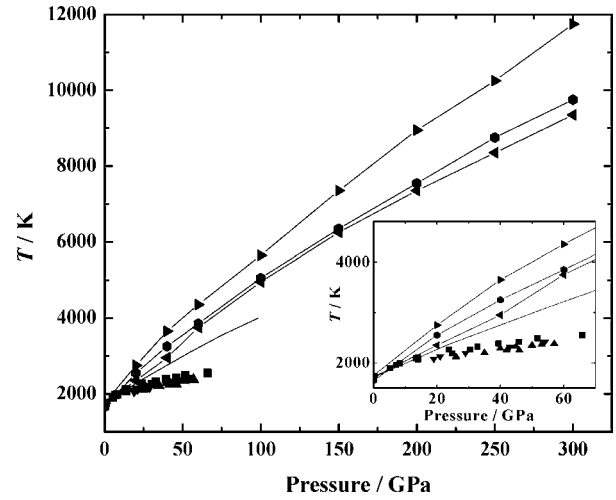

Figure 4. Experimentally determined melting temperatures of Ni at 0 GPa in ref 3, □, compared with the DAC measurements of Lazor et al. in ref 2, ■; ▲, Errandonea et al. in ref 4; and ▼, Japel et al. in ref 7. −, theoretical simulated melting curves by Ross et al. in ref 18. Melting temperatures at different pressures obtained with the two-phase approach and simulations containing: right-pointing triangle, 512; left-pointing triangle, 1000; and ●, 1728 atoms in this work.

Table 1. Melting Temperatures of Ni with 1000 Atoms under High Pressure

P (GPa)	T_m (K)
0	1725 ± 25
60	3750 ± 50
100	4950 ± 50
150	6250 ± 50
200	7350 ± 50
250	8350 ± 50
300	9350 ± 50

experimental and theoretical data for Ni about ultrapressure melting temperatures, we hope that this piece of data can provide a useful benchmark on the melting properties of the high pressure of nickel.

Comparing the melting curves of Ta and Mo with the DAC melting results, we wonder if there are enormous discrepancies with the DAC at higher pressure in these transition metals. The melting of Ta were simulated using the solid−liquid coexistence phase MD simulations[17] and the Z-method MD simulations,[19] whereas Mo[14] uses the coexistence phase density functional theory (DFT) MD calculations. From Figure 5, it is interesting to see that the Ta and Mo melting curves exhibit common features with the melting curves for Ni—a rapid increase of melting temperature with pressure in the theoretical calculations and the calculated melting temperatures are much higher than the DAC results[4] at high pressure. Recently, an experiment[8] was used to solve the problem of large divergence of the theoretical values and previous experimental values of tantalum. From in situ X-ray diffractions, the tantalum samples were modified under intense laser irradiation, and then the anomalous low melting curve was not found.

Solid−liquid transitions begin with nucleation, and then the nucleus of the daughter phase reaches a critical size. In the phase transition proceeding, the Gibbs energy barrier should be overcome to the formation of the nucleus of the daughter phase. The nucleation-induced superheating can be automatically eliminated in the two-phase simulation, as the interface assists in the nucleation for the melting or crystallization process.[23] Also, we can apply the hysteresis method to avoid superheating. We treat Ni as an ideal solid and liquid in our simulations and

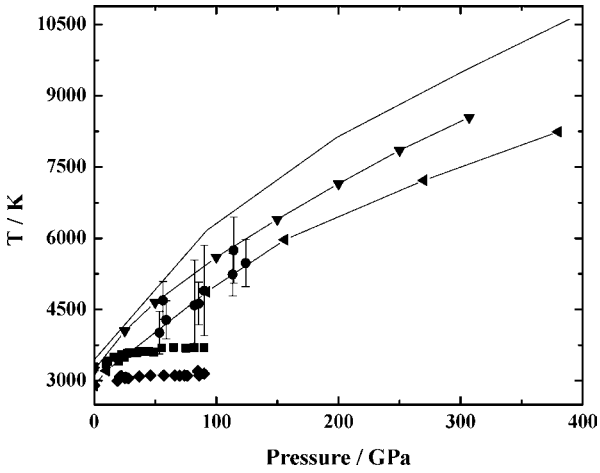

Figure 5. MD predicted melting curves of Ta: ▼, in ref 17 and —, in ref 19; compared with DAC data for Ta: ■, in ref 4 and ●, in ref 8. MD predicted melting curves of Mo: left-pointing triangle, in ref 14; compared with DAC data for Mo: □, in ref 4.

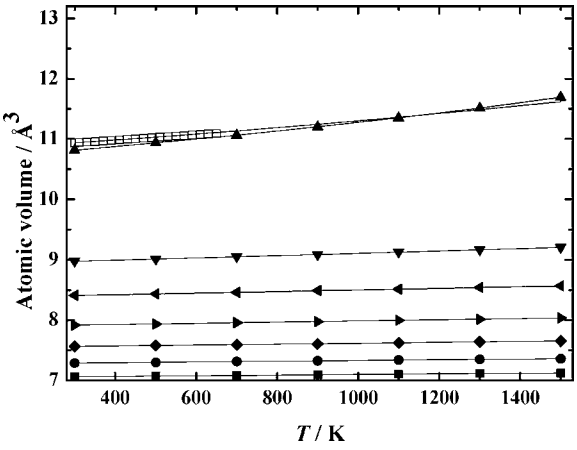

Figure 7. Isobars of fcc Ni at different pressures: ▲, 0 GPa; ▼, 60 GPa; left-pointing triangle, 100 GPa; right-pointing triangle, 150 GPa; ◆, 200 GPa; ●, 250 GPa; and ■, 300 GPa; the previous calculations of Wang et al. in ref 46, □, and Pavlovic et al. in ref 47, —, are shown for comparison.

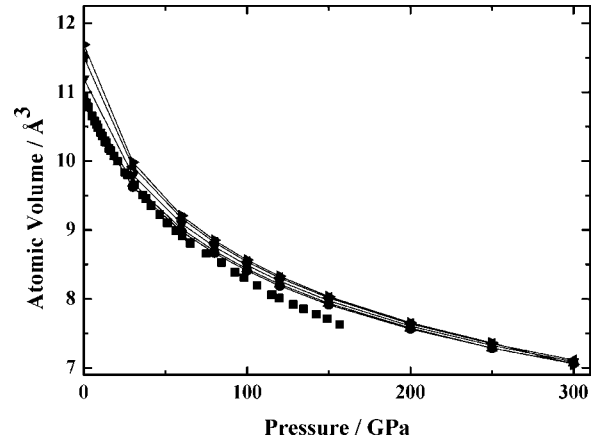

Figure 6. Isotherms of fcc Ni at various temperatures: ●, 300 K; ▲, 500 K; ▼, 900 K; left-pointing triangle, 1300 K; and right-pointing triangle, 1500 K; experiment results in ref 45, ■, are shown for comparison.

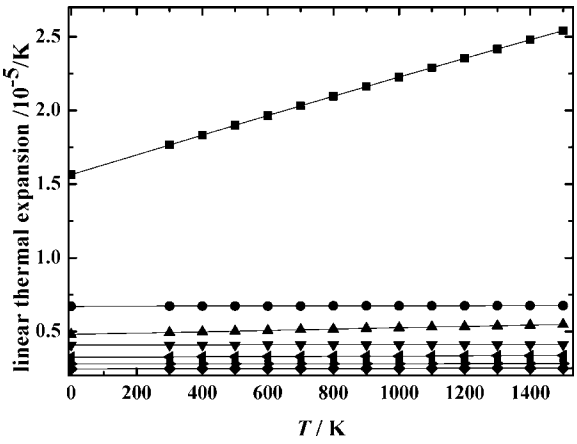

Figure 8. Coefficient of linear thermal expansivity of fcc structured Ni as a function of temperature at different pressures: ■, 0 GPa; ●, 60 GPa; ▲, 100 GPa; ▼, 150 GPa; left-pointing triangle, 200 GPa; right-pointing triangle, 250 GPa; and ◆, 300 GPa.

ignore the local structures; this may overestimate the melting temperature to some extent. The presence of icosahedral short-range order (ISRO) was confirmed in Ni.[38,39] For the metals ranging from Zr and Ta to Mo,[18,40,41] we can observe the ISRO in DFT-MD simulations. Ross et al.[18] mentioned that for Ni, Ta, and Mo metals with partially filled *d* bands Peierls−Jahn−Teller distortions are responsible for a high level of liquid frustration leading to low melting slopes. The partially filled *d* shell has the capacity to form locally preferred structures, which lowers the free energy of the liquid so that T_m becomes lower. The conflict with the DAC result and all of the theoretical results still exists. Apart from the above reasons, another reason may be the existence of new phases in both solid and liquid Ni under high pressures. A possible resolution of the conflict has emerged recently for Mo.[42−44] Up to now, the high-pressure melting curve of Ni still remains inconclusive, so more experimental measurements and theoretical calculations are urgently necessary to further determine the phases and then the whole melting curve.

3.2. Thermal Equation of State (EOS). To determine the thermal EOS of Ni, the MD simulation is performed on an NPT ensemble at various temperature and pressure values. The calculated isothermal compression curves are compared with the experimental calculation[45] in Figure 6, in which the 300 K isotherm is in excellent agreement with experiment values at low pressure but deviates a little from experiment at high pressure. The dispersion in our simulations might be due to that we only considered a pure crystal in our simulation, whereas impurities do exist in the experimental samples and there are also some experimental limitations. The isothermal compressibilities of Ni show a decrease with pressure, reflecting the increasing repulsion of the electronic clouds as the pressure goes up. At different temperatures, the response of Ni is similar. In Figure 7, our calculations are consistent with other theoretical calculations[46,47] at 0 GPa. The isobaric expansivity increases with temperature, which is the general trend for solids. It is clear that the isobaric expansivity exhibits the same tendency at different pressures.

As an important physical quantity, the thermal expansion of a solid is closely related to the anharmonicity of lattice vibrations and the anharmonic nature of the interatomic forces. In MD simulations, the linear coefficient of thermal expansion can be obtained directly from the definition $\alpha_l = (1/a)(\partial a/\partial T)|_P$, where *a* is the lattice constant. In Figure 8, we plot the thermal expansion coefficient as a function of temperature at different pressures. Our calculated thermal expansion coefficient is $1.79 \cdot 10^{-5}$ K^{-1} at ambient conditions, consistent with the experimental value of $1.23 \cdot 10^{-5}$ K^{-1}.[48] As pressure rises, the thermal expansion coefficient decreases rapidly at each temperature. The effects of temperature are increasingly suppressed,

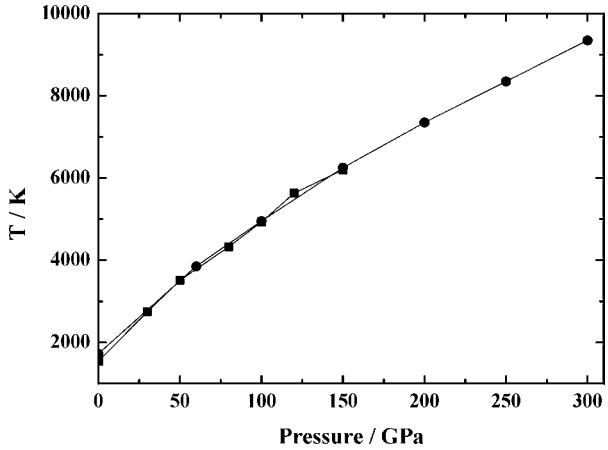

Figure 9. High-pressure melting points of nickel: ■, prediction from the hysteresis method and ●, two-phase simulation in this work.

and thus the thermal expansion converges to a nearly constant value in the limit of high pressure and temperature. This is mainly because the anharmonic effects become less important at high pressure. With the increasing pressure, the volume of the solid is decreased, and the atoms come closer to each other, increasing the depth of the potential energy well and reducing the anharmonic nature of the potential energy curve at high temperature.

3.3. Solid−Liquid Interfacial Tension. In the NPT ensemble, we heated the 500 ($5 \times 5 \times 5$) Ni atoms incrementally up to high temperature and then cooled them at fixed pressure. A phase transition was detected by a discontinuous change of the volume, and T_+ and T_- are obtained (Figure 3). We applied two methods to determine the melting temperature: the solid−liquid coexistence phase simulation and the hysteresis method. In the present simulations, one noted that the hysteresis approach and the two-phase method can also eliminate the superheating, and the melting curves from the two methods are nearly identical (Figure 9). We adopted the hysteresis method in the following discussion.

In hysteresis process, we deduced θ_c^+ and θ_c^- from the obtained T_+, T_-, and T_m, and then the value of β can be determined by eq 7. We obtained ΔH_m and ΔV from the enthalpy and volume difference between the solid and the liquid at T_m. Once these values are obtained, we can determine the solid−liquid tension γ_{sl}. The values of γ_{sl} calculated from (T_m, ΔH_m, T_+) and (T_m, ΔH_m, T_-) are essentially the same and are consistent with other studies.[34,49,50] Physical properties of nickel in the hysteresis process at various pressures are shown in Table 2 and have been plotted in Figure 10. The solid−liquid tension $\gamma_{sl} \approx 0.197$ J·m^{-2} at ambient pressure is presented in Table 2, which is in good agreement with the result of Zykova-Timan et al.[30] but is slightly smaller than the value of Hoyt et al.[29] From Figure 10, we can see that all of the pressure dependence of physical properties under high pressure cannot be described as linear relations. It is noticeable that θ_c^+ and θ_c^- are respectively 1.22 ± 0.02 and 0.72 ± 0.02 for Ni and keep constant regardless of pressure. All of the physical properties can be described as polynomials perfectly, which are shown as follows

$$\Delta V = 0.011 - 2.86864 \cdot 10^{-5} P + 5.54233 \cdot 10^{-8} P^2 \quad (7)$$

Table 2. Physical Properties of Nickel in the Hysteresis Process at Various Pressures[a]

	T_+	T_-	T_m				ΔV	ΔH_m	γ_{sl}
P	K	K	K	θ_c^+	θ_c^-	β	nm^3	kJ·mol^{-1}	J·m^{-2}
0	1850	1150	1541	1.200	0.746	1.476	0.0117	14.28	0.197
30	3350	1950	2744	1.220	0.716	1.829	0.0103	22.99	0.384
50	4250	2550	3507	1.211	0.727	1.664	0.0099	26.91	0.460
80	5350	2950	4327	1.236	0.681	2.122	0.0096	33.81	0.634
100	6150	3250	4930	1.247	0.659	2.353	0.0093	34.46	0.709
120	6850	4050	5632	1.216	0.719	1.744	0.0088	39.87	0.765
150	7550	4450	6200	1.217	0.717	1.757	0.0082	41.80	0.861

[a] Superheating melting point (T_+), supercooling melting point (T_-), melting point (T_m), ratio of maximum superheating and supercooling (θ_c^+ and θ_c^-), nucleation barrier parameter (β), average volume per atom (ΔV), enthalpy change per unit volume between solid and liquid states at melting point (ΔH_m), and solid-liquid interfacial tension (γ_{sl}) are displayed.

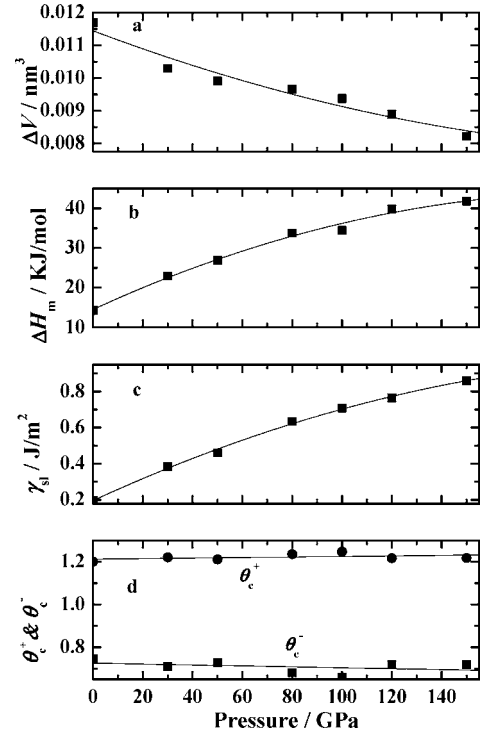

Figure 10. Physical properties of nickel in the hysteresis process: (a) average volume per atom (ΔV), (b) heat of fusion (ΔH_m), (c) planar interfacial energy (γ_{sl}), and (d) superheating and supercooling ($\theta_c^{\pm}$) as a function of pressure.

$$\Delta H_m = 14.527 + 0.2864P - 0.69441 \cdot 10^{-4} P^2 \quad (8)$$

$$\gamma_{sl} = 0.196 + 0.00633P - 1.2685 \cdot 10^{-5} P^2 \quad (9)$$

$$\theta_c^+ = 1.212 + 1.23694 \cdot 10^{-4} P \quad (10)$$

$$\theta_c^- = 0.725 - 2.1671 \cdot 10^{-4} P \quad (11)$$

4. Conclusions

In summary, we employed MD to compute the melting properties, thermal EOS, and the solid−liquid interfacial tension of the fcc structure of Ni. Applying the two-phase MD, we obtained the melting curve of Ni at (0 to 300) GPa with a different numbers of atoms. We found 1000 atoms can reach a convergence of the melting temperature. Meanwhile, we have compared the two techniques commonly used to calculate the

melting curve of a material with classical MD, namely, the hysteresis (one-phase) approach and the solid−liquid coexistence (two-phase) approach. These methods strongly reduced the overheating, and they are identical over the range of pressure examined. At high pressure, the discrepancy between our results and DAC results still exists. The anomalous phenomena can be found in transition metals such as Ta and Mo and so on. So more experimental and theoretical research is urgently necessary to solve the conflict and determine the melting curve.

Using the superheating−supercooling hysteresis method, we also calculated the solid−liquid interfacial energy of nickel. This method has been successful applied to many materials, so we predicted the solid−liquid interfacial energy of nickel in the range (0 to 150) GPa. Under high pressure, the solid−liquid interfacial tension γ_{sl} can be described as a second-order polynomial relation. Moreover, the thermal EOS has been investigated, and the linear thermal expansivity as a function of temperature has been also obtained successfully.

Literature Cited

(1) Hixson, R. S.; Boness, D. A.; Shaner, J. W.; Moriarty, J. A. Acoustic Velocities and Phase Transitions in Molybdenum under Strong Shock Compression. *Phys. Rev. Lett.* **1989**, *62*, 637.

(2) Lazor, P.; Shen, G.; Saxena, S. K. Laser-Heated Anvil Cell Experiments at High Pressure: Melting Curve of Nickel up to 700 kbar. *Phys. Chem. Miner.* **1993**, *20*, 86.

(3) Kittel, C. *Introduction to Solid State Physics*; Wiley: New York, 1996.

(4) Errandonea, D.; Schwager, B.; Ditz, R.; Boehler, R.; Ross, M. Systematics of transition-metal melting. *Phys. Rev. B* **2001**, *63*, 132104.

(5) Errandonea, D.; Somayazulu, M.; Usermann, D. H.; Mao, H. K. Melting of tantalum at high pressure determined by angle dispersive X-ray diffraction in a double-sided laser-heated diamond-anvil cell. *J. Phys.: Condens. Matter* **2003**, *15*, 7635.

(6) Errandonea, D. Comment on 'Theoretical solid and liquid state shock Hugoniots of Al, Ta, Mo and W'. *J. Phys.: Condens. Matter* **2004**, *16*, 8801.

(7) Japel, S.; Schwager, B.; Boehler, R.; Ross, M. Melting of Copper and Nickel at High Pressure: The Role of *d* Electrons. *Phys. Rev. Lett.* **2005**, *95*, 167801.

(8) Dewaele, A.; Mezouar, M.; Guignot, N.; Loubeyre, P. High melting points of tantalum in a Laser-Haeted Diamond Anvil Cell. *Phys. Rev. Lett.* **2010**, *104*, 255701.

(9) Moriarty, J. A.; Belak, J. F.; Rudd, R. E.; Soderlind, P.; Streitz, F. H.; Yang, L. H. Quantum-based atomistic simulation of materials properties in transition metals. *J. Phys.: Condens. Matter* **2002**, *14*, 2825.

(10) Luo, S. N.; Ahrens, T. J.; Cagin, T.; Strachan, A.; Goddard, W. A., III; Swift, D. C. Maximum superheating and undercooling: Systematics, molecular dynamics simulations, and dynamic experiments. *Phys. Rev. B* **2003**, *68*, 134206.

(11) Belonoshko, A. B.; Simak, S. I.; Kochetov, A. E.; Johansson, B.; Burakovsky, L.; Preston, D. L. High-Pressure Melting of Molybdenum. *Phys. Rev. Lett.* **2004**, *92*, 195701.

(12) Strachan, A.; Cagin, T.; Gülseren, O. G.; Mukherjee, S.; Cohen, R. E.; Goddard, W. A., III. First principles force field for metallic tantalum. *Modell. Simul. Mater. Sci. Eng.* **2004**, *12*, S445.

(13) Verma, A. K.; Rao, R. S.; Godwal, B. K. Theoretical solid and liquid state shock Hugoniots of Al, Ta, Mo and W. *J. Phys.: Condens. Matter* **2004**, *16*, 4799.

(14) Cazorla, C.; Gillan, M. J.; Taioli, S.; Alfè, D. Ab initio melting curve of molybdenum by the phase coexistence method. *J. Chem. Phys.* **2007**, *126*, 194502.

(15) Luo, S. N.; Swift, D. C. On high-pressure melting of tantalum. *Physica B* **2007**, *388*, 139.

(16) Taioli, S.; Cazorla, C.; Gillan, M. J.; Alfè, D. Melting curve of tantalum from first principles. *Phys. Rev. B* **2007**, *75*, 214103.

(17) Liu, Z. L.; Cai, L. C.; Chen, X. R.; Jing, F. Q. Molecular dynamics simulations of the melting curve of tantalum under pressure. *Phys. Rev. B* **2008**, *77*, 024103.

(18) Ross, M.; Boehler, R.; Errandonea, D. Melting of transition metals at high pressure and the influence of liquid frustration: The late metals Cu, Ni, and Fe. *Phys. Rev. B* **2007**, *76*, 184117.

(19) Burakovsky, L.; Chen, S. P.; Preston, D. L.; Belonoshko, A. B.; Rosengren, A.; Mikhaylushkin, A. S.; Simak, S. I.; Moriarty, J. A. High-pressure−High-temperature Polymorphism in Ta: Resolving an Ongoing Experimental Controversy. *Phys. Rev. Lett.* **2010**, *104*, 255702.

(20) Cagin, T.; Qi, Y.; Li, H.; Kimura, Y.; Ikeda, H.; Johnson, W. L.; Goddard, W. A., III. Calculation of mechanical, thermodynamic and transport properties of metallic glass formers. *MRS Symp. Ser.* **1999**, *554*, 43–48.

(21) Belonoshko, A. B.; Ahuja, R.; Johansson, B. Quasi-*Ab Initio* Molecular Dynamic Study of Fe Melting. *Phys. Rev. Lett.* **2000**, *84*, 16.

(22) Luo, F.; Chen, X. R.; Cai, L. C.; Wu, Q. Thermoelastic properties of nickel from molecular dynamic simulations. *J. At. Mol. Sci.* **2010**, *2*, 10.

(23) Morris, J. R.; Wang, C. Z.; Ho, K. M.; Chan, C. T. Melting line of aluminum from simulations of coexisting phases. *Phys. Rev. B* **1994**, *49*, 3109.

(24) Morris, J. R.; Song, X. The melting lines of model systems calculated from coexistence simulations. *J. Chem. Phys.* **2002**, *116*, 9352.

(25) Ogitsu, T.; Schwegler, E.; Gygi, F.; Galli, G. Melting of Lithium Hydride under Pressure. *Phys. Rev. Lett.* **2003**, *91*, 175502.

(26) Belonoshko, A. B.; Dubrovinsky, L. S. Molecular dynamics of NaCl (B1 and B2) and MgO (B1) melting; two-phase simulation. *Am. Mineral.* **1996**, *81*, 303.

(27) Harfuji, K.; Tsuchiya, T.; Kawamura, K. Molecular dynamics simulation for evaluating melting point of wurtzite-type GaN crystal. *J. Appl. Phys.* **2004**, *96*, 2501.

(28) Koči, L.; Ahuja, R.; Belonoshko, A. B.; Johansson, B. Study of the high-pressure helium phase diagram using molecular dynamics. *J. Phys.: Condens. Matter* **2007**, *19*, 016206.

(29) Hoyt, J. J.; Asta, M.; Karma, A. Method for Computing the Anisotropy of the Solid-Liquid Interfacial Free Energy. *Phys. Rev. Lett.* **2001**, *86*, 5530.

(30) Zykova-Timan, T.; Rozas, R. E.; Horbach, J.; Binder, K. Computer simulation studies of finite-size broadening of solid-liquid interfaces: from hard spheres to nickel. *J. Phys.: Condens. Matter* **2009**, *21*, 464102.

(31) Smith, W.; Forrester, T. R.; Todorov, I. T.; Leslie, M. *The DL_POLY_2 user manual, version 2.17*; The Council for the Central Laboratory of Research Councils: Daresbury Laboratory, Warrington, Cheshire, UK, 2006.

(32) Berendsen, H. J. C.; Postma, J. P. M.; Gunsteren, W. V.; DiNola, A.; Haak, J. R. Molecular dynamics with coupling to an external bath. *J. Chem. Phys.* **1984**, *81*, 3684.

(33) Essmann, U.; Perera, L.; Berkowitz, M. L.; Darden, T.; Lee, H.; Pederson, L. G. A smooth particle mesh Ewald method. *J. Chem. Phys.* **1995**, *103*, 8577.

(34) Luo, S. N.; Strachan, A.; Swift, D. C. Nonequilibrium melting and crystallization of a model Lennard-Jones system. *J. Chem. Phys.* **2004**, *120*, 11640.

(35) Luo, S. N.; Ahrens, T. J. Superheating systematics of crystalline solids. *Appl. Phys. Lett.* **2003**, *82*, 1836.

(36) Zheng, L.; Luo, S. N.; Thompson, D. L. Molecular dynamic simulations of melting and glass transition of nitromethane. *J. Chem. Phys.* **2006**, *124*, 154504.

(37) Belonoshko, A. B. Atomistic Simulation of Shock Wave-Induced Melting in Argon. *Science* **1997**, *278*, 1475.

(38) Jakse, N.; Pasturel, A. Ab initio molecular dynamics simulations of local structure of supercooled Ni. *J. Chem. Phys.* **2004**, *120*, 6124.

(39) Jakse, N.; Pasturel, A. Molecular-dynamics study of liquid nickel above and below the melting point. *J. Chem. Phys.* **2005**, *123*, 244512.

(40) Jakse, N.; Pasturel, A. Local Order of Liquid and Supercooled Zirconium by *Ab Initio* Molecular Dynamics. *Phys. Rev. Lett.* **2003**, *91*, 195501.

(41) Jakse, N.; Bacq, O. L.; Pasturel, A. Prediction of the local structure of liquid and supercooled tantalum. *Phys. Rev. B* **2004**, *70*, 174203.

(42) Belonoshko, A. B.; Burakovsky, L.; Chen, S. P.; Johansson, B.; Mikhaylushkin, A. S.; Preston, D. L.; Simak, S. I.; Swift, D. C. Molybdenum at High Pressure and Temperature: Melting from Another Solid Phase. *Phys. Rev. Lett.* **2008**, *100*, 135701.

(43) Cazorla, C.; Alfè, D.; Gillan, M. J. Comment on "Molybdenum at High Pressure and Temperature: Melting from Another Solid Phase". *Phys. Rev. Lett.* **2008**, *101*, 049601.

(44) Mikhaylushkin, A. S.; Simak, S. I.; Burakovsky, L.; Chen, S. P.; Johansson, B.; Preston, D. L.; Swift, D. C.; Belonoshko, A. B. Mikhaylushkin et al. Reply. *Phys. Rev. Lett.* **2008**, *101*, 049602.

(45) Dewaele, A.; Torrent, M.; Loubeyre, P.; Mezouar, M. Compression curves of transition metals in the Mbar range: Experiments and projector augmented-wave calculations. *Phys. Rev. B* **2008**, *78*, 104102.

(46) Pavlovic, A. S.; Babu, V. S.; Seehra, M. S. High-temperature thermal expansion of binary alloys of Ni with Cr, Mo and Re: a comparison with molecular dynamics simulations. *J. Phys.: Condens. Matter* **1996**, *8*, 3139.

(47) Wang, T.; Zhu, J. Z.; Mackay, R. A.; Chen, L. Q.; Liu, Z. K. Modeling of Lattice Parameter in the Ni-Al System. *Metall. Mater. Trans. A* **2004**, *35A*, 2318.

(48) Kollie, T. G. Measurement of the thermal-expansion coefficient of nickel from 300 to 1000 K and determination of the power-law constants near the Curie temperature. *Phys. Rev. B* **1977**, *16*, 4872.
(49) Lu, K.; Li, Y. Homogeneous Nucleation Catastrophe as a Kinetic Stability Limit for Superheated Crystal. *Phys. Rev. Lett.* **1998**, *80*, 4474.
(50) Luo, S. N.; Strachan, A.; Damian, C. S. Deducing solid-liquid interfacial energy from superheating or supercooling: application to H_2O at high pressures. *Modell. Simul. Mater. Sci. Eng.* **2005**, *13*, 321.

Received for review July 1, 2010. Accepted September 17, 2010. We would like to acknowledge support by the National Natural Science Foundation of China (Grant Nos. 10776022 and 10776029) and by the Specialized Research Fund for the Doctoral Program of Higher Education under Grant No. 20090181110080.

JE1007058